Polym. Bull. (2012) 68:1341–1355
DOI 10.1007/s00289-011-0626-5

ORIGINAL PAPER

A novel castor oil-based polyurethane/layered zirconium phosphonate nanocomposites: preparation, characterization, and properties

Jun Ma · Changhua Liu · Rui Li · Lina Zhu · Haixia Wu

Received: 1 March 2011 / Revised: 23 June 2011 / Accepted: 3 September 2011 /
Published online: 9 September 2011
© Springer-Verlag 2011

Abstract A new type of layered zirconium glycine-*N*,*N*-dimethylphosphonate (ZGDMP), with the functional groups –COOH, has been prepared and characterized by X-ray diffraction (XRD), scanning electron microscope (SEM) and transmission electron microscopy (TEM). Situ polymerization method was employed to prepare castor oil-based polyurethane/layered zirconium phosphonate (PU/ZGDMP-*n*) nanocomposite films. The structure and morphology of ZGDMP in PU matrix have been characterized by XRD, SEM, TEM, and Fourier transform infrared spectroscopy. The results show that the morphology and properties of PU-based nanocomposites greatly depend on the functional groups –COOH because of the chemical reactions and physical interactions involved. The tensile test shows that the tensile strength and elongation at break for the nanocomposite films increase with the loading of ZGDMP as compared to those of the virgin PU.

Keywords Interaction · Nanocomposite · Polyurethane · Zirconium glycine-*N*,*N*-dimethylphosphonate

Introduction

In recent years, bio-based materials obtained from renewable resources have gained increasing interest for wide applications [1–4] from a social, environmental, and energy standpoint, with the increasing emphasis on issues concerning waste disposal and depletion of non-renewable resources [5]. Vegetable oil is most abundant, annually renewable natural resources available in large quantities from various oilseeds, such as castor, palm, and canola oils [6–10]; they are relatively low cost

J. Ma · C. Liu (✉) · R. Li · L. Zhu · H. Wu
College of Chemistry and Chemical Engineering, Southwest University, Chongqing 400715, People's Republic of China
e-mail: chliu@swu.edu.cn

materials which offer a priori possibility of biodegradation. Castor oil is a relatively inexpensive source of secondary hydroxyl groups and a triglyceride of fatty acids with ricinoleic acid being the major constituent [11], which has the general structure with $R \equiv (C_2)_7CH{=}CHCH_2CHOH(CH_2)_5CH_3$ for ricinoleic acid, and it has been used as a polyol to synthesize cost-effective and biodegradable polyurethane (PU). However, disadvantages with the use of castor oil include low hydroxyl number leading to inherently low modulus materials, a sluggish rate of curing of the secondary hydroxyl groups [12] and structural irregularity due to steric hindrance offered by the long pendant fatty acid chains during urethane formation, resulting in low tensile strength [13]. In order to improve the mechanical strength of castor oil-based PU, various types of filler, like clay [14], CNTs [15], TiO_2 [16], and silicate [17] used as an effective strategy have been incorporated into PU to prepare nanocomposites. The results demonstrated that homogeneous dispersion of fillers in PU matrix significantly improved the performance of the nanocomposites.

In this study, we have designed and prepared zirconium phosphate derivatives, zirconium glycine-*N*,*N*-dimethylphosphonate (ZGDMP) $Zr[(O_3PCH_2)_2NCH_2COOH]\cdot H_2O$ (Scheme 1), containing –COOH functional groups by direct reaction of tetravalent zirconium ions with organophosphoric acids *N*,*N*-bis(phosphonomethyl)-glycine ($(H_2O_3PCH_2)_2NCH_2COOH$). The –COOH functional groups onto the surface of the layers not only can react with the isocyanic group but also could improve the compatibility with polar PU matrix. This would endow the nanocomposites with better properties due to the formation of stronger chemical bonding and hydrogen bonding, resulting stronger interfacial adhesion between ZGDMP and PU matrix [18].

Scheme 1 Structure scheme of ZGDMP

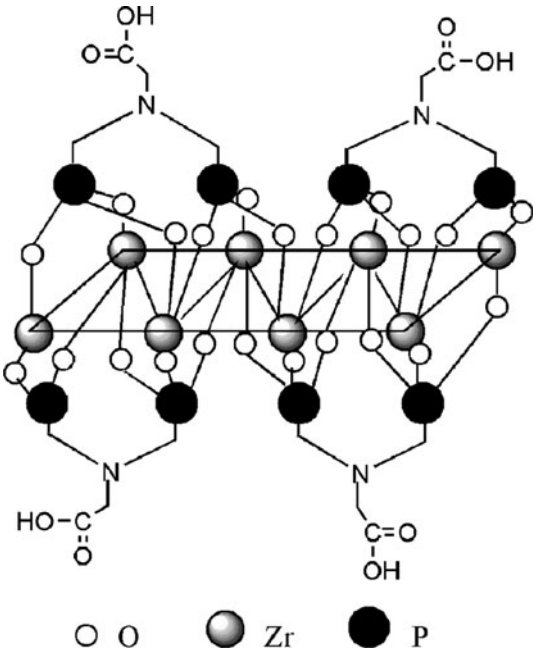

The objective of this article is to discuss the formation of the chemical bonding and hydrogen bonding between matrix and fillers on effect of the structure and properties of nanocomposites. The structure, thermal, and mechanical properties of the ZGDMP nanocomposite films are studied by Fourier transform infrared (FT-IR) spectroscopy, wide-angle X-ray diffraction (XRD), scanning electron microscope (SEM), transmission electron microscopy (TEM), thermogravimetric analysis (TGA), and tensile testing.

Experimental

Materials

All the chemicals and reagents used were of analytical grade. $ZrOCl_2 \cdot 8H_2O$ was provided by Kelong Chemical Co. (Chongqing, China). 2,4-Toluene diisocyanate (2,4-TDI) was purchased from Kelong Chemical Co.(Chongqing, China) and used without further purification. Castor oil, chemical grade with a 4.94 wt% content of hydroxyl groups and hydroxyl value of 163, was obtained from Daxing Chemical Co. (Ningbo, China) and dehydrated at 100 °C under 20 mmHg for 1 h. *N*,*N*-bis(phosphonomethyl)-glycine ($(H_2O_3PCH_2)_2NCH_2COOH$, DMPG) was synthesized according to literature [19]. Phosphoric acid was purchased from Chongqing Beibei Chemical Reagent Factory (Chongqing, China).

Synthesis of ZGDMP

ZGDMP was prepared according to the following procedure. A solution of DMPG (9.12 g, 0.04 mol) in 50 mL water was added into $ZrOCl_2 \cdot 8H_2O$ (6.45 g, 0.02 mol) in 50 mL water with vigorous stirring and refluxing for 24 h. The precipitate was filtered and washed using de-ionized water to pH $= 5 \sim 6$, and dried in vacuo at 60 °C.

Film preparation

PU/ZGDMP-*n* nanocomposite films were prepared by a prepolymer mixing process. PU prepolymer was synthesized in a 250 mL three-necked flask equipped with a condenser, thermostat, mechanical stirrer, and a pressure equalizing dropping funnel. 30.0 g of 2,4-TDI was firstly charged into the flask. 59.0 g of castor oil was dropped into the flask within 40 min and stirred at 60 °C for 2 h to get the PU prepolymer. The value of [NCO]/[OH] was predetermined theoretically to be 1.05. After the preparation of the prepolymer, it was cooled down to room temperature. Then, 3.0 g of PU prepolymer was mixed with a stoichiometric amount of ZGDMP. After 30 min, 0.25 g of 1,4-butanediol as chain-extending agent in tetrahydrofuran (THF) was added into the solution, and then the solution was mixed after fully dissolution. The solution was cast onto glass plate after stirred at room temperature for 1 h. After slow solvent evaporation at room temperature in atmosphere, it was cured at 80 °C for 4 h. The films were vacuum-dried at room temperature for 3 days

Table 1 Codes of the samples and the thermal analysis of PU/ZGDMP-*n* composite films measured from the TGA and DSC

Code	PU/ ZGDMP-0	PU/ ZGDMP-1	PU/ ZGDMP-2	PU/ ZGDMP-3	PU/ ZGDMP-4	PU/ ZGDMP-5
ZGDMP (wt%)	0	0.2	0.4	0.6	0.8	1.0
T_{max} (°C)	308.34	309.21	309.72	312.61	308.45	309.24
IDT (°C)	252.93	258.65	260.46	264.95	263.16	259.75
T_g (°C)	22.70	23.90	24.00	25.50	23.67	22.60
20% loss (°C)	297.57	304.49	304.50	306.80	304.28	309.00
50% loss (°C)	364.08	372.10	372.10	372.23	376.71	377.82
D (nm) ((001) direction for ZGDMP)	–	17.61	17.39	12.20	20.49	21.50

The results of XRD calculated crystal size *D* of (001) direction for ZGDMP in the composites

and then were used for the measurements [20]. By adjusting ZGDMP loading to 0, 0.2, 0.4, 0.6, 0.8, and 1.0 wt%, respectively, a series of the films with a thickness of around 0.1 mm were prepared and coded as PU/ZGDMP-*n* (where *n* represented the ZGDMP loading). To serve as experimental controls, the neat PU film was obtained through the same fabrication process, which was coded as PU/ZGDMP-0. The codes of samples were listed in Table 1.

Characterization

FT-IR spectroscopy of the complex was recorded with a Nicolet 170SX (Madison, WI, USA) FT-IR spectrometer in the wavelength range of 4000–725 cm^{-1} in the attenuated total reflection mode.

XRD patterns of the samples were carried out with a XRD-3D, PuXi (Beijing, China) X-ray diffractometer under the following conditions: Nickel filtered Cu$K\alpha$ radiation ($\lambda = 0.15406$ nm) at a voltage of 36 kV and current of 20 mA. The scanning rate was 4°/min in the angular range of 3°–50° (2θ).

The PU/ZGDMP-*n* nanocomposite films were fractured in liquid nitrogen, and the cross sections were mounted on SEM stubs with double-sided adhesive tape, and then coated with gold in a 13.3 Pa vacuum degree. A SEM (S-3000, HITACHI, Japan) was used to observe the morphologies of cross sections of the films at an accelerating voltage of 5 kV. The morphology of the pristine ZGDMP was observed at an accelerating voltage of 20 kV (S-4800, HITACHI, Japan).

TEM micrographs were obtained with a TEM (JEM-100CXII, Japan) at an accelerating voltage of 80 kV. Ultrathin sections were microtomed at room temperature.

TGA and differential thermogravimetry (DTG) analyses of the PU/ZGDMP-*n* films were carried out on a TA-STDQ600 (TA Instruments Inc, New Castle, USA). The thermograms were acquired between room temperature and 500 °C at a heating rate of 10 °C/min. Nitrogen was used as the purge gas at a flow rate of 20 mL/min. An empty pan Al_2O_3 was used as a reference.

Differential scanning calorimetry (DSC) analysis of the PU/ZGDMP-0, PU/ZGDMP-1, PU/ZGDMP-3, and PU/ZGDMP-*n* nanocomposite films was carried on a NETZSCH DSC 200 F3 (Netzsch Co, Selb/Bavaria, Germany). Nitrogen at a rate of 20 mL/min was used as the purge gas. Aluminum pans containing 2 to 3 mg of film were sealed with pierced lid using the DSC sample press. All samples were preheated with a scan rate of 20 °C/min over a temperature range of −30 to 110 °C.

The tensile strength and elongation at break of the films were determined using a Micro-electronics Universal Testing Instrument Model Sans 6500 (Shenzhen Sans Testing Machine Co. Ltd, Shenzhen, China) according to the Chinese standard method (GB 13022-91). The films were cut into 10-mm wide and 100-mm long strips and mounted between cardboard grips (150 × 300 mm) using adhesive so that the final area exposed was 10 × 50 mm. The cross-head speed was 10 mm/min. All measurements were performed on three specimens and averaged.

Results and discussion

Structural analysis

The FT-IR spectra of ZGDMP, ZGDMP after grafting on 2,4-TDI (2,4-TDI/ZGDMP), and product of ZGDMP and 2,4-TDI prepared in the presence of 1-butanol (2,4-TDI/ZGDMP/1-butanol) were shown in Fig. 1a to prove the chemical bonding between ZGDMP and 2,4-TDI. The infrared spectrum of ZGDMP (Fig. 1a (A)) presented the following bands: 1690, 1423, and 1026 cm^{-1}, which were attributed to the C=O stretching of COOH groups, O–H bending vibration of COOH, and P–O stretching, respectively. For the 2,4-TDI/ZGDMP (Fig. 1a (B)), the band at 2276 cm^{-1} was typical N=C=O vibrations. The band centered at 1598 cm^{-1} was due to the C–H vibrations on the benzene ring. Moreover, the peak of O–H bend vibrations of COOH in ZGDMP (Fig. 1a (A)) almost disappeared in the 2,4-TDI/ZGDMP (Fig. 1a (B)). In addition, there are several strong bands between 1628 and 1648 cm^{-1} (relating to C=O), between 1519 and 1563 cm^{-1} (relating to NH) as well as between 1221 and 1253 cm^{-1} (also relating to NH), suggesting the formation of the amide linkage and the N=C=O group of 2,4-TDI reacted with COOH group on the surface of ZGDMP. As compared to 2,4-TDI/ZGDMP, the peak in the spectrum of 2,4-TDI/ZGDMP/1-butanol (Fig. 1a (C)) assigned to free –NCO groups located at 2276 cm^{-1} disappeared, indicating that the –OH groups of 1-butanol react more easily than the –COOH groups of ZGDMP with –NCO groups. The absorption peak of C=O stretching vibration of urethane linkage was at 1725 cm^{-1}. Moreover, the peak at 1217 cm^{-1} was due to C–C=O peaks. And the bands at 1169 and 997 cm^{-1} were attributed to the *asymmetrical stretching vibration* and symmetrical stretching vibration of C–O–C groups, respectively. These proved the formation of urethane linkage. However, the bands of the amide linkage which were similar to that of 2,4-TDI/ZGDMP also appeared in the spectrum of 2,4-TDI/ZGDMP/1-butanol. All these results indicated that both ZGDMP and 1-butanol can react with –NCO groups of 2,4-TDI.

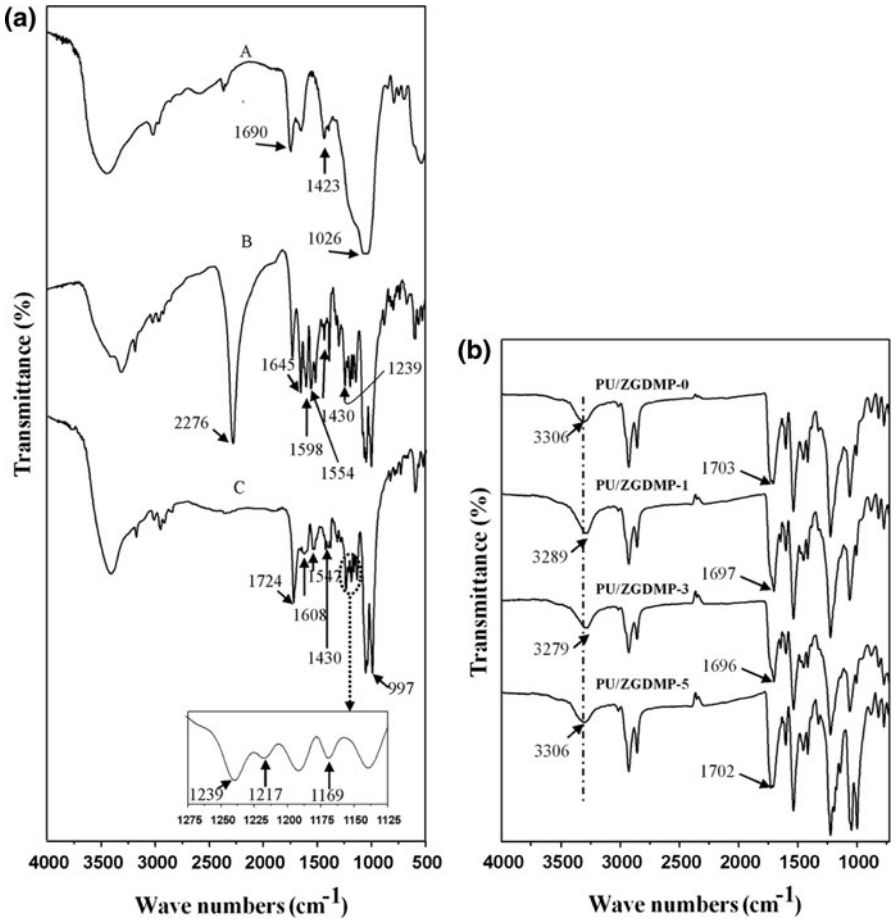

Fig. 1 **a** FT-IR spectra of ZGDMP (*A*), 2,4-TDI/ZGDMP (*B*), and 2,4-TDI/ZGDMP/1-butanol (*C*) and **b** FT-IR spectra of PU/ZGDMP-0, PU/ZGDMP-1, PU/ZGDMP-3, PU/ZGDMP-5 nanocomposite films

The FT-IR spectra of PU/ZGDMP-*n* nanocomposite films are shown in Fig. 1b. For the neat PU film, the band centered at 3306 cm^{-1} is due to the self-associate bonded N–H stretching [21, 22]. A sharp peak near 1703 cm^{-1} was due to the C=O stretching vibrations. The band at 1597 cm^{-1} was the C=C bending. The peak at 1219 cm^{-1} was due to C–C=O peaks [23–26]. The characteristic absorption peak at 1703 cm^{-1} and the NH stretching ($\nu_{NH} \sim 3306$ cm^{-1}) absorption of neat PU film shifted to lower wave numbers in the nanocomposite films, respectively, [25, 27, 28] for PU/ZGDMP-1 and PU/ZGDMP-3 nanocomposite films with an increase of ZGDMP loading, and original inter- and intra-molecular hydrogen bonding involved in films were destroyed due to two interfacial interaction ways. The most important way was that the N=C=O of PU prepolymer reacted with the COOH of ZGDMP leading to the formation of chemical bonding shown in the Fig. 1a which was more stronger than hydrogen bonding (shown in Scheme 2). In this way, it

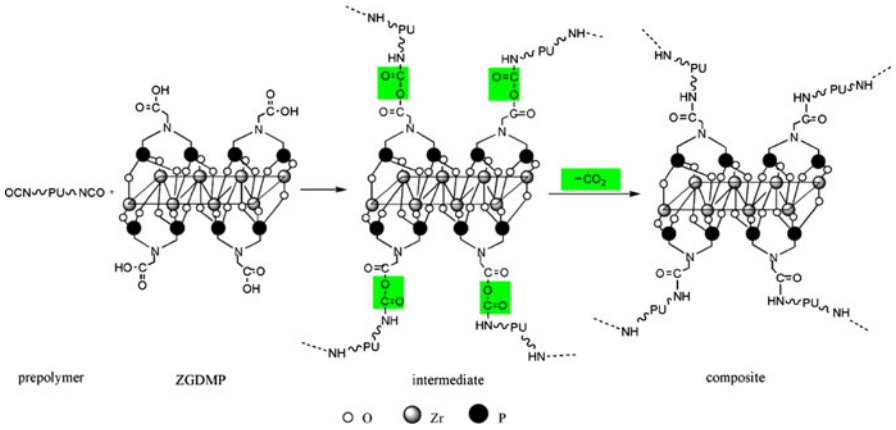

Scheme 2 Reaction pathway for the reaction of ZGDMP with PU prepolymer

could have stronger interfacial interaction between them, which led to increased properties of nanocomposite films. The other way was that the hydrogen bonding was formed by the hydroxyl groups, amino groups of PU with carboxyl of ZGDMP, if so it will have great interaction between PU and ZGDMP.

The XRD patterns of ZGDMP and PU/ZGDMP-*n* films are shown in Fig. 2. It could be obviously seen that ZGDMP (A) prepared according to previous descriptive method was semi crystalline due to the absence of hydrofluoric acid (HF) and short reactive time. Wu et al. [29] have successfully prepared crystalline ZGDMP with the interlayer distance of 1.273 nm ($2\theta = 6.940°$) and the crystal size D of 16.16 nm for ZGDMP in the presence of complexing agent HF and 120 h reactive time. The characteristic diffraction peak was splited into two peaks around at $2\theta = 6.21°$, 5.65° with two phases due to strong preferred orientation and steric demands. As shown in Fig. 2, the neat PU film (PU/ZGDMP-0) showed a broad diffraction commencing from 12 to 28 in 2θ with lower magnitude. This indicated the amorphous nature of PU, similar to other works [20, 22, 30]. The PU/ZGDMP-*n* films showed the different XRD patterns as the neat PU film [31–33]. The characteristic diffraction peaks in the (001) direction for ZGDMP were found in the nanocomposite films. From the theoretical prediction, with the increase of the ZGDMP loading, the intensity of the peaks in the (001) direction in the nanocomposites should become stronger and stronger. However, disagreement was obtained between experimental data and the theoretical prediction. The experimental data in Fig. 2 showed that the full width at half-maximum (FWHM) for the (001) direction of PU/ZGDMP-3 nanocomposite was larger than other nanocomposites. According to Scherrer's law ($D = k\lambda/\beta\cos\theta$) [34–36], the crystal size D of (001) direction for ZGDMP in the composites was calculated and listed in Table 1. With the increase of ZGDMP loading, the minimum of D value (12.20 nm) appeared in PU/ZGDMP-3 composite. This could be explained that the ZGDMP particles were dispersed best in PU/ZGDMP-3 among all these composites, which resulted in the best mechanical properties for PU/ZGDMP-3 composite. It can be

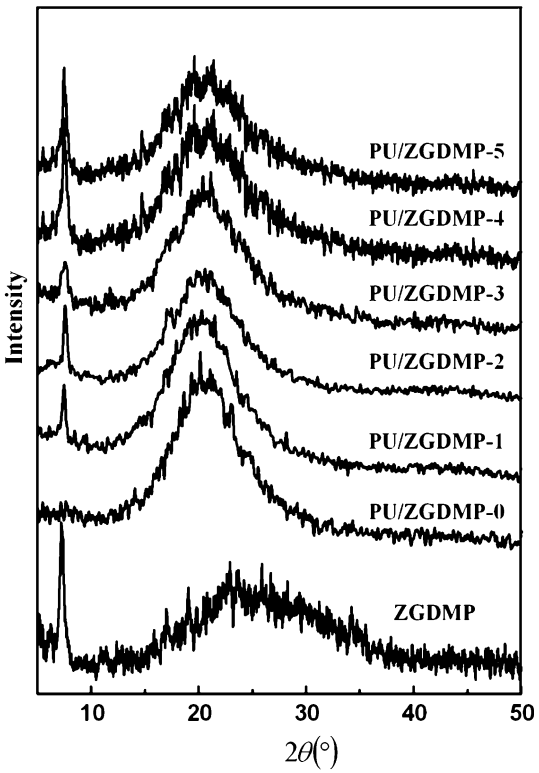

Fig. 2 XRD patterns of ZGDMP and PU/ZGDMP-*n* nanocomposite films

explained that there is the most strong interaction in PU/ZGDMP-3 nanocomposite film between PU and ZGDMP, leading to suppress the crystallization of ZGDMP.

Morphological image analysis

Examination of ZGDMP powers and the fractured surface of PU/ZGDMP-*n* nanocomposites, which were broken at liquid nitrogen, was carried out by SEM, and Fig. 3 shows the images of the ZGDMP and the nanocomposites filled with 0.0, 0.2, 0.4, 0.6, 0.8, and 1.0 wt% ZGDMP, respectively. It was noted that ZGDMP exhibited layer structure and irregular thin sheets with particle sizes varying approximately between 5 and 10 μm. It was also seen that ZGDMP presented semi crystalline, which was proven by XRD pattern (Fig. 2). As compared to the matrix, the morphology of ZGDMP can be easily identified. The white substance in the images corresponds to ZGDMP on the fractured surface of the nanocomposites. Well dispersed ZGDMP in the nanocomposites can be observed in PU/ZGDMP-1, PU/ZGDMP-2, and PU/ZGDMP-3, while PU/ZGDMP-4 and PU/ZGDMP-5 show that ZGDMP aggregates in the nanocomposites with higher filler loading. As shown in PU/ZGDMP-1, PU/ZGDMP-2, and PU/ZGDMP-3, a homogeneous distribution of the filler embedded in the PU matrix was observed, implying that ZGDMP layers are dispersed well and regularly in PU matrix in PU/ZGDMP-1, PU/ZGDMP-2, and

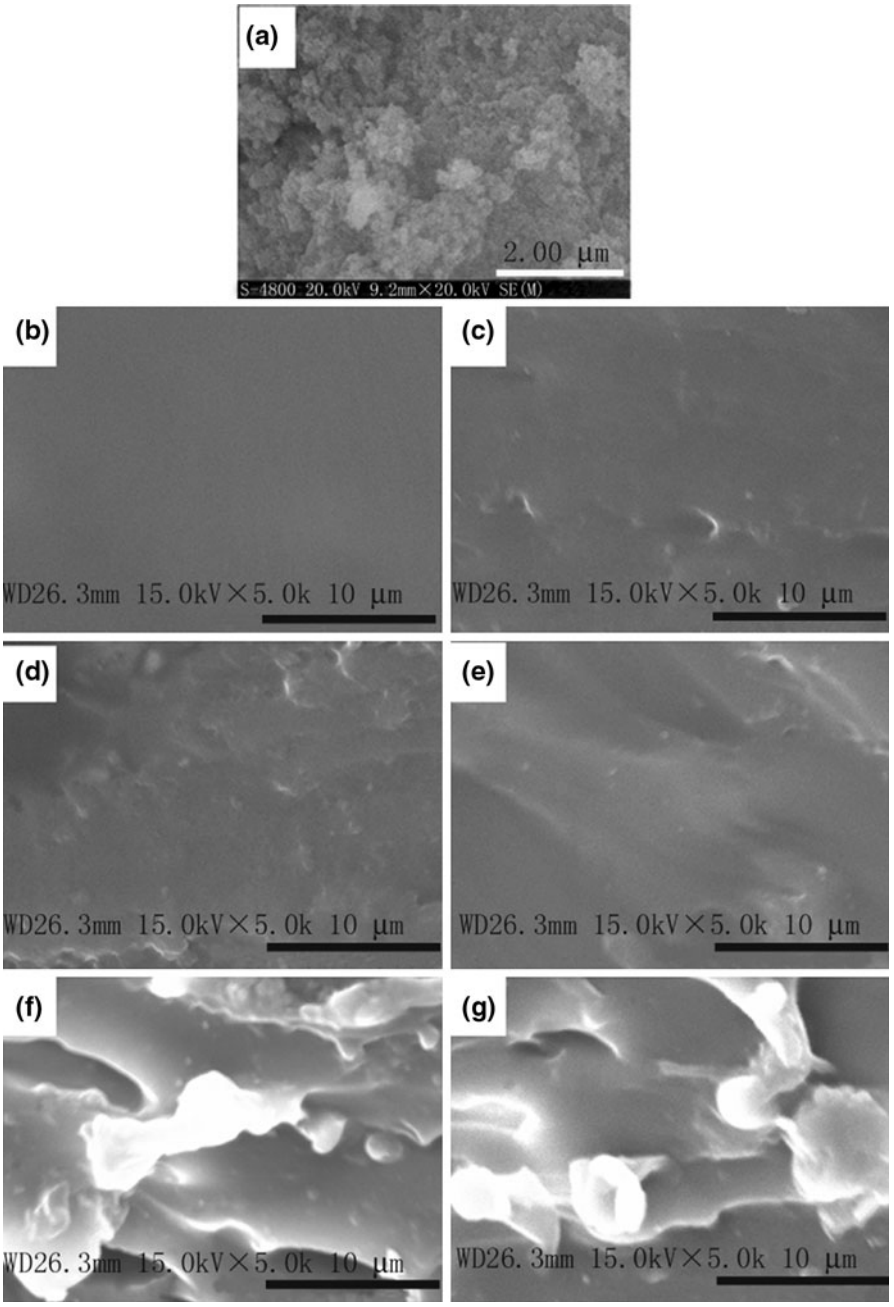

Fig. 3 SEM micrographs of pristine ZGDMP (**a**) at ×20000 magnification and fracture surface for the films: PU/ZGDMP-0 (**b**), PU/ZGDMP-1 (**c**), PU/ZGDMP-2, (**d**), PU/ZGDMP-3 (**e**), PU/ZGDMP-4 (**f**), and PU/ZGDMP-5 (**g**) at ×5000 magnification

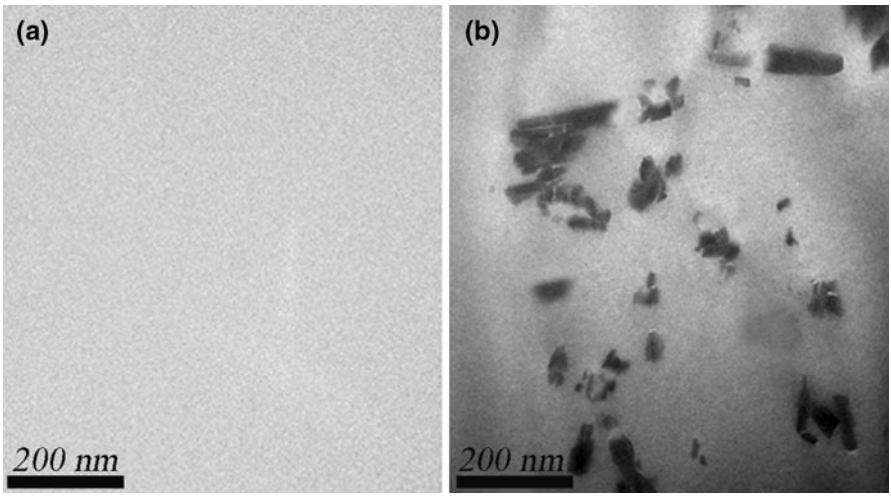

Fig. 4 TEM micrographs of **a** PU matrix and **b** PU/ZGDMP-3 nanocomposite film containing 0.6 wt% ZGDMP

PU/ZGDMP-3, which benefit the formations of intermolecular hydrogen bonding and chemical bonding, increasing the molecular interfacial interaction. Such an even and uniform distribution of the fillers in the PU matrix played an important role in improving the mechanical performance of the films as discussed later. In the PU/ZGDMP-4 and PU/ZGDMP-5, it was found that different sizes of ZGDMP aggregates or chunks on the surface of the PU. This can explain why the mechanical properties become worse when the ZGDMP loadings are 0.8 and 1.0 wt%. Two factors may affect this phenomenon. First, the interaction of PU chains cause ZGDMP layers appended on PU chains, this prevents the ZGDMP to agglomerate. Second, there are plenty of –COOH bonding in the interlayer space of ZGDMP, in high concentration the –COOH may not react with N=C=O completely, which result in worse properties in high concentration.

TEM micrographs of the PU matrix and PU/ZGDMP-3 nanocomposite are shown in Fig. 4. The neat PU exhibits a uniform microstructure (In Fig. 4a). In Fig. 4b, the dark particles correspond to the individual ZGDMP platelets in the PU matrix. The layered ZGDMP in the size ranges of 20–50 nm are randomly and well dispersed in the PU matrix, which resulted from strong interaction between ZGDMP and PU.

Thermal analyses

The thermal stability of the neat PU and their nanocomposites films was studied by TGA, shown in Fig. 5a. First, the weight loss between 217 and 336 °C was attributed to the breaking of urethane bond. Second, the decomposition stage of PU lies in the range from 336 to 480 °C, due to castor oil molecules resulted in a faster rate of weight loss. This was according to the literature [20]. The summary of TGA results was listed in Table 1. T_{max} was the temperature corresponding to maximum

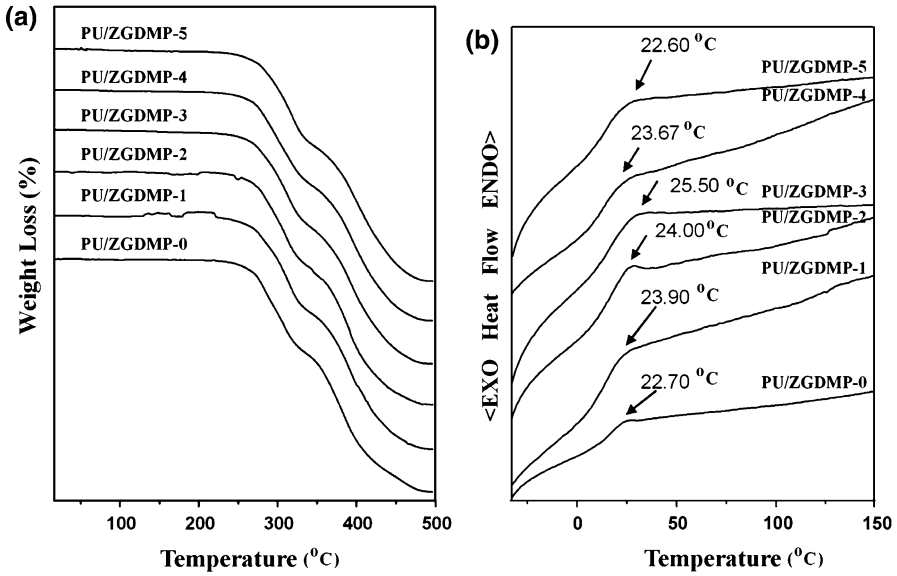

Fig. 5 **a** TGA curves of PU/ZGDMP-*n* nanocomposite films and **b** DSC curves of PU/ZGDMP-*n* nanocomposite films

rate of degradation. It was seen that T_{max} of neat PU films were 308.34 °C. For all the complexes, it was seen that the T_{max} of PU was improved after adding ZGDMP into PU matrix (Table 1). As degradation temperature at 50% loss weight was concerned, the thermal degradation temperature of PU was improved by about 8 °C after adding 0.6 wt% ZGDMP, due to the fact that the ZGDMP have well dispersion and stronger interfacial interaction with PU matrix in PU/ZGDMP-3. Moreover, the degradation temperature at 20% loss weight and the initial decomposition temperature (IDT) were improved after adding ZGDMP into PU matrix. Figure 5b shows the DSC curves for the composite films. One glass transitions were detected in the nanocomposite films. Meanwhile, the T_g temperature associated with the glass transition of PU for the nanocomposite films PU/ZGDMP-1, PU/ZGDMP-2, PU/ZGDMP-3, and PU/ZGDMP-4 were found to be 23.90, 24.00, 25.50, and 23.67 °C, which were higher than that of the pure PU film (22.70 °C). The improved T_g can be explained through the reduced mobility of the PU chains in the nanocomposite, which benefit from the interfacial interaction of the PU molecule with the ZGDMP. On one hand, the –COOH of ZGDMP could react with the –NCO of PU prepolymer (Scheme 2). On the other hand, the hydrogen bond could also be formed through –COOH on the surface of ZGDMP with –NH– and –CO– of the PU prepolymer. These two factors led to the reduced chain mobility, and consequently the glass transition temperature for nanocomposites was improved [37].

Mechanical properties

Mechanical properties of the films incorporated with different loadings of ZGDMP were investigated by tensile testing. From the stress–strain curves in Fig. 6a, two

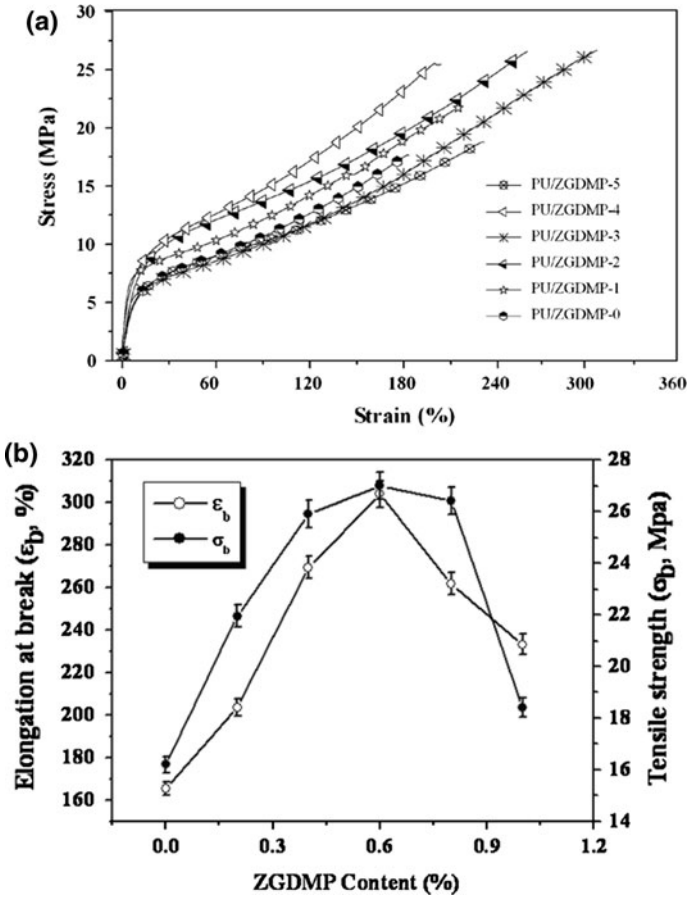

Fig. 6 **a** Stress–strain curves of PU/ZGDMP-*n* nanocomposite films and **b** the mechanical properties of PU/ZGDMP-*n* nanocomposite films

regions of deformation behavior of all samples were observed. In the First Newton Area, the stress increased rapidly with increasing strain at low strains, and the stress increased regularly at higher strain with the strain increasing up to the break of the films in the High-elastic zone. It is worth noting that all of the nanocomposite films displayed clearly elastomeric behavior. The area of under the stress–strain curve can be used as a measurement of the material toughness. The relatively large area of the films PU/ZGDMP-2 and PU/ZGDMP-3 indicated a character of toughened rubber. The tensile strength and elongation at break were determined and displayed in Fig. 6b. It was observed that ZGDMP loadings influenced the mechanical properties of the composite films. It is known that –COOH groups of ZGDMP can react with the active N=C=O groups of the prepolymer leading to the formation of chemical bonds shown in Fig. 2a. Moreover, –COOH groups on the surface of the layered ZGDMP can interact with the $–NH_2$ and –C=O groups. Hence, stronger interfacial interactions occurred between ZGDMP and PU with increasing ZGDMP loadings.

It was observed that with the loadings varied from 0 to 0.6 wt%, the tensile strength (σ_b) was significantly enhanced from 16.19 to 27.02 MPa with the increasing elongation at break (ε_b) from 165.35 to 304.00%. When the ZGDMP loading was more than 0.6 wt%, the tensile strength and the elongation at break of the films decreased. This can be explained by the fact that ZGDMP is the rigid filler, which is responsible for the enforcing effect. Meanwhile, the decrease of the mechanical strength of the films with more than 0.6 wt% may be attributed to the aggregation of excess filler in PU matrix. In combination with the result of SEM, it can be summarized that an optimum amount of ZGDMP exists for an effective enhancement of the mechanical properties of the nanocomposites. The interfacial interaction of ZGDMP with PU at lower amount in nanocomposite was preferable, indicating the best interfacial interaction between the PU and ZGDMP due to the formed chemical bonding and stronger hydrogen bonding [26]. Hence, it results in the good mechanical properties. However, with higher amount of ZGDMP loadings, the agglomerates of ZGDMP can damage the structure of the matrix, which results in decreased mechanical property.

Conclusion

In this study, the effect of ZGDMP loading and interfacial interaction with PU on the mechanical and structural properties of the PU/ZGDMP-*n* nanocomposites was investigated. The result from FT-IR indicated that the –COOH groups on the surface of the layered ZGDMP can react with the active N=C=O groups of the prepolymer and interact with the $–NH_2$ and –C=O groups of PU through hydrogen bonding. These results from tensile testing and TG proved that the functional ZGDMP with –COOH groups can enhance the tensile strength and the thermal stability through chemical reactions and hydrogen bondings. Consequently, the functionalization of layered zirconium phosphonate can improve the compatibility and interfacial interaction between fillers and PU matrix.

References

1. Hatti-Kaul R, Törnvall U, Gustafsson L, Börjesson P (2007) Industrial biotechnology for the production of bio-based chemicals a cradle-to-grave perspective. Trends Biotechnol 25:119–124
2. Campanella A, Bonnaille LM, Wool RP (2009) Polyurethane foams from soyoil-based polyols. J Appl Polym Sci 112:2567–2578
3. Deka H, Karak N (2009) Bio-based hyperbranched polyurethanes for surface coating applications. Prog Org Coat 66:192–198
4. Fritzen-Garcia MB, Oliveira IRWZ, Zanetti-Ramos BG, Fatibello-Filho O, Soldi V, Pasa AA (2009) Carbon paste electrode modified with pine kernel peroxidase immobilized on pegylated polyurethane nanoparticles. Sens Actuators B Chem 139:570–575
5. Corcuera MA, Rueda L, Fernandez d'Arlas B, Arbelaiz A, Marieta C, Mondragon I et al (2010) Microstructure and properties of polyurethanes derived from castor oil. Polym Degrad Stab 95:2175–2184
6. Sharna V, Kundu PP (2008) Condensation polymers from natural oils. Prog Polym Sci 33:1199–1215

7. Xu Y, Petrovic Z, Das S, Wilkes GL (2008) Morphology and properties of thermoplastic polyurethanes with dangling chains in ricinoleate-based soft segments. Polymer 49:4248–4258
8. Hablot E, Zheng D, Bouquey M, Avérous L (2008) Polyurethanes based on castor oil: kinetics, chemical, mechanical and thermal properties. Macromol Mater Eng 293:922–929
9. Petrovic ZS (2008) Polyurethanes from vegetable Oils. Polym Rev 48:109–155
10. Javni I, Zhang W, Petrovic ZS (2003) Effect of different isocyanates on the properties of soy-based polyurethanes. J Appl Polym Sci 88:2912–2916
11. Somani KP, Kansara SS, Patel NK, Rakshit AK (2003) Castor oil based polyurethane adhesives for wood-to-wood bonding. Int J Adhes Adhes 23:269–275
12. Bai S, Khakhar DV, Nadkarni VM (1997) Mechanical properties of simultaneous interpenetrating polymer networks of castor oil based polyurethane and polystyrene. Polymer 38:4319–4323
13. Mortley A, Bonin HW, Bui VT (2007) Synthesis and properties of radiation modified thermally cured castor oil based polyurethanes. Nucl Instrum Methods Phys Res B 265:98–103
14. Herrera-Alonso JM, Marand E, Little JC, Cox SS (2009) Transport properties in polyurethane/clay nanocomposites as barrier materials: effect of processing conditions. J Membr Sci 337:208–214
15. Zhang R, Dowden A, Deng H, Baxendale M, Peijs T (2009) Conductive network formation in the melt of carbon nanotube/thermoplastic polyurethane composite. Compos Sci Technol 69:1499–1504
16. Sabzi M, Mirabedini SM, Zohuriaan-Mehr J, Atai M (2009) Surface modification of TiO_2 nanoparticles with silane coupling agent and investigation of its effect on the properties of polyurethane composite coating. Prog Org Coat 65:222–228
17. Finnigan B, Martin D, Halley P, Truss R, Campbell K (2004) Morphology and properties of thermoplastic polyurethane nanocomposites incorporating hydrophilic layered silicates. Polymer 45: 2249–2260
18. Sun LY, Boo WJ, Sue HJ, Clearfield A (2007) Preparation of α-zirconium phosphate nanoplatelets with wide variations in aspect ratios. New J Chem 31:39–43
19. Moedritzer K, Irani RR (1966) The direct synthesis of α-aminomethylphosphonic acids. Mannich-type reactions with orthophosphorous acid. J Org Chem 31:1603–1607
20. Zhou Q, Zhang LN, Zhang M, Wang B, Wang S (2003) Miscibility, free volume behavior and properties of blends from cellulose acetate and castor oil-based polyurethane. Polymer 44:1733–1739
21. Nakamura K, Nishimura Y, Zetterlund P, Hatakeyama T, Hatakeyama H (1996) TG-FTIR studies on biodegradable polyurethanes containing mono- and disaccharide components. Thermochim Acta 282–283:433–441
22. Liu J, Ma D, Li Z (2002) FTIR studies on the compatibility of hard–soft segments for polyurethane–imide copolymers with different soft segments. Eur Polym J 38:661–665
23. Stuart L, Cooper AV (1966) Properties of linear elastomeric polyurethanes. J Appl Polym Sci 10:1837–1844
24. Koberstein JT, Gancarz I (1986) The effects of morphological transitions on hydrogen bonding in polyurethanes: preliminary results of simultaneous DSC-FTIR experiments. J Appl Polym Sci B Polym Phys 24:2487–2498
25. Kuan HC, Ma CM, Chang WP, Yuen SM, Wu HH, Lee TM (2005) Synthesis, thermal, mechanical and rheological properties of multiwall carbon nanotube/waterborne polyurethane nanocomposite. Compos Sci Technol 65:1703–1710
26. John J, Bhattacharyal M, Turner RB (2002) Characterization of polyurethane foams from soybean oil. J Appl Polym Sci 86:3097–3107
27. Berta M, Lindsay C, Pans G, Camino G (2006) Effect of chemical structure on combustion and thermal behavior of polyurethane elastomer layered silicate nanocomposites. Polym Degrad Stab 91:1179–1191
28. Semenzato S, Lorenzetti A, Modesti M, Ugel E, Hrelja D, Besco S (2009) A novel phosphorus polyurethane FOAM/montmorillonite nanocomposite: preparation, characterization and thermal behavior. Appl Clay Sci 44:35–42
29. Wu H, Liu C, Chen J, Chang PR, Chen Y, Anderson DP (2009) Starch-based nanocomposites reinforced with layered zirconium phosphonate. Carbohydr Polym 77:358–364
30. Salahuddin N, Abo-El-Enein SA, Selim A, Salah El-Dien O (2010) Synthesis and characterization of polyurethane/organo-montmorillonite nanocomposites. Appl Clay Sci 47:242–248
31. Furuakwa MJ (1994) Property-structure relationships of polyurethane elastomers: improvement of hydrolytic stability and thermal stability. Appl Polym Sci Appl Polym Symp 53:61–76
32. Furukawa M (1997) Hydrolytic and thermal stability of novel polyurethane elastomers. Angew Macromol Chem 252:33–43

33. Furukawa M, Shiiba T, Murata S (1999) Mechanical properties and hydrolytic stability of polyesterurethane elastomers with alkyl side groups. Polymer 40:1791–1798
34. Kar-Gupta R, Venkatesh TA (2008) Electromechanical response of piezoelectric composites: effects of geometric connectivity and grain size. Acta Mater 56:3810–3823
35. Shen L, Chen Z (2007) An investigation of grain size and nitrogen-doping effects on the mechanical properties of ultrananocrystalline diamond films. Int J Solids Struct 44:3379–3392
36. Byun SC, Jeong YJ, Park JW, Kim SD, Ha HY, Kim WJ (2006) Effect of solvent and crystal size on the selectivity of ZSM-5/Nafion composite membranes fabricated by solution-casting method. Solid State Ion 177:3233–3243
37. Kuljanin J, Čomor MI, Djoković V, Nedeljković JM (2006) Synthesis and characterization of nanocomposite of polyvinyl alcohol and lead sulfide nanoparticles. Mater Chem Phys 95:67–71